Supplement of Atmos. Chem. Phys., 25, 10987–11002, 2025
https://doi.org/10.5194/acp-25-10987-2025-supplement

Atmospheric Chemistry and Physics
Open Access
EGU

Supplement of

Aerosol hygroscopicity over the South-East Atlantic Ocean during the biomass burning season – Part 2: Influence of sea salt and burning conditions on CCN hygroscopicity

Haochi Che et al.

Correspondence to: Haochi Che (haochi.che@geo.uio.no) and Lu Zhang (luzhang@envs.au.dk)

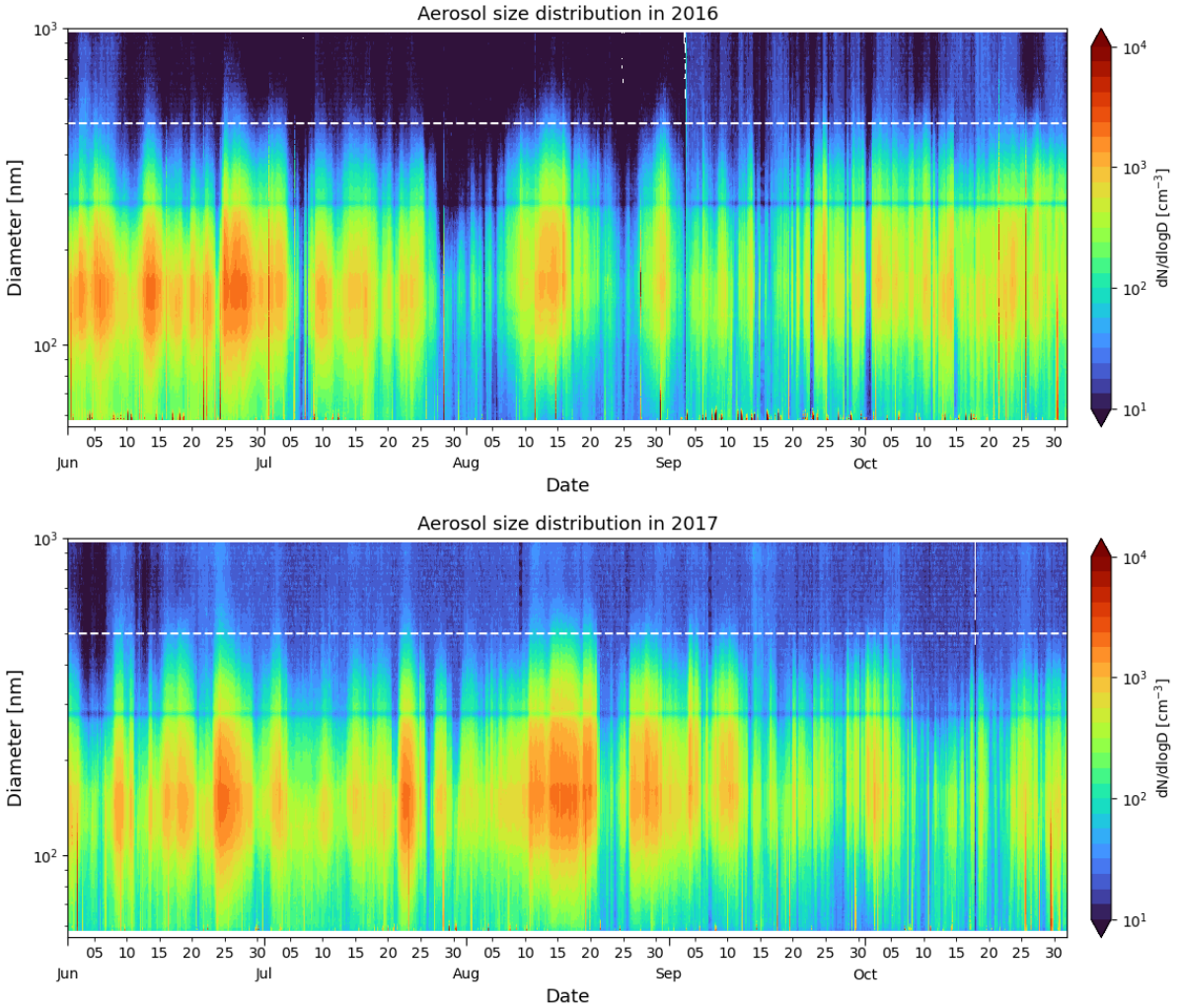

Figure S1. Aerosol size distribution measured by the UHSAS during the fire seasons of 2016 and 2017. The plot is based on hourly averaged data. The white dashed line at 500 nm marks the upper size limit of the SMPS.

S1. Sensitivity of κ-based Cutoff Diameter Selection

In this study, the aerosol number concentration from the SMPS (N_{SMPS}) was integrated from 31 nm to 1000 nm, using an activation diameter corresponding to $\kappa = 0.6$ at 1% supersaturation (31 nm). While this choice is well-suited for 2017 conditions—where measured κ values support the assumption—the 2016 data exhibited lower κ values (around 0.3), raising the question of whether using a uniform cutoff might introduce biases in N_{SMPS} and the derived κ between 2016 and 2017.

The critical activation diameter (D_{50}) corresponding to $\kappa = 0.6$ is approximately 31 nm at 1% supersaturation, while for $\kappa = 0.3$, D_{50} increases to around 39 nm at the same supersaturation. The difference in N_{SMPS} values integrated from 31 nm versus 39 nm therefore reflects the aerosol number concentration between 31 and 39 nm. Based on the mean aerosol size distribution during the 2016 fire season, this size range contained an average of 17 particles/cm³. Given that the total mean N_{SMPS} during this period was approximately 277 particles/cm³, this difference accounts for only a small fraction of the total particle concentration.

To evaluate the practical impact on CCN–SMPS consistency, we compared the correlation between CCN concentration at 1% supersaturation ($N_{CCN1\%}$) and integrated SMPS concentrations using two lower cutoff sizes: 31 nm (N31) and 39 nm (N39), focusing on June 2016 data. As shown in Figure S2, the two correlations are nearly identical, indicating that the choice of cutoff size does not significantly affect the CCN counting correction.

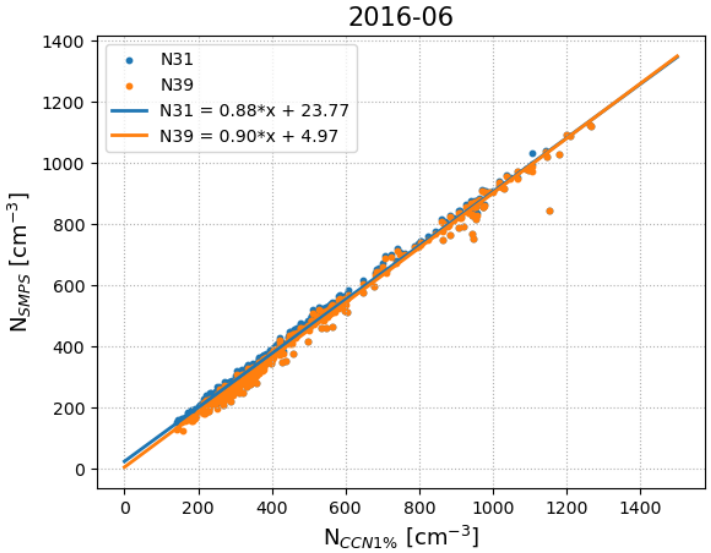

Figure S2. Correlation between N_{SMPS} and $N_{CCN1\%}$. N_{SMPS} is calculated by integrating the aerosol size distribution from two lower size limits (31 nm and 39 nm) up to 1000 nm.

Furthermore, we evaluated the impact on the derived hygroscopicity parameter κ at 0.1% supersaturation. Figure S3 shows that κ values calculated using N31 (κ_{31}) and N39 (κ_{39}) differ only slightly. The most noticeable differences occur in the higher κ range, where κ κ_{39} tends to be lower than κ_{31}Within the typical κ range observed in 2016 (0.2 to 0.4), switching from N_{31} to N_{39} results in an average difference of less than 0.08.

Given the small magnitude of these differences and the importance of maintaining a consistent methodology across the entire campaign, we have chosen to retain the N_{31}-based integration. This approach ensures consistency and comparability between the 2016 and 2017 datasets while introducing only negligible uncertainty.

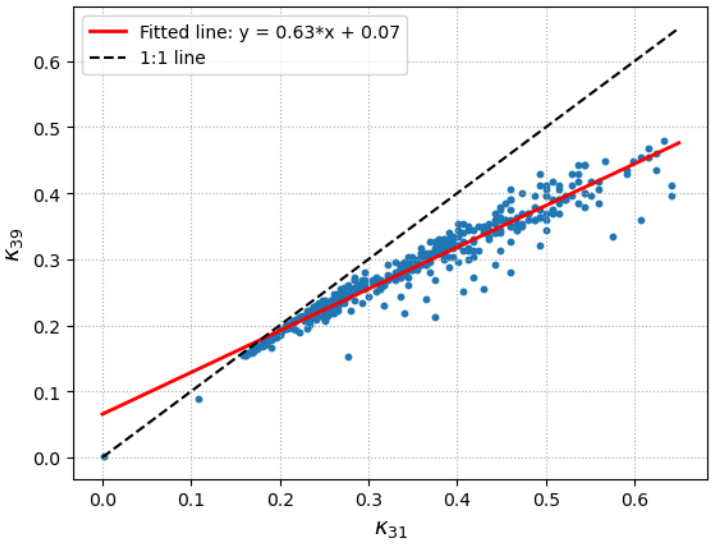

Figure S3. Correlation between κ_{31} and κ_{39} in June 2016.

S2. Correlation shifts between $N_{CCN1\%}$ and N_{SMPS}

In the main manuscript, we identified two distinct correlation patterns (Type 1 and Type 2) between the CCN concentration at 1% supersaturation ($N_{CCN1\%}$) and the integrated aerosol number concentration from the SMPS (N_{SMPS}, 31–1000 nm), suggesting a potential instrumental change during the LASIC campaign. To investigate the cause of this shift, we analyzed the aerosol time series, presented in Figure S4.

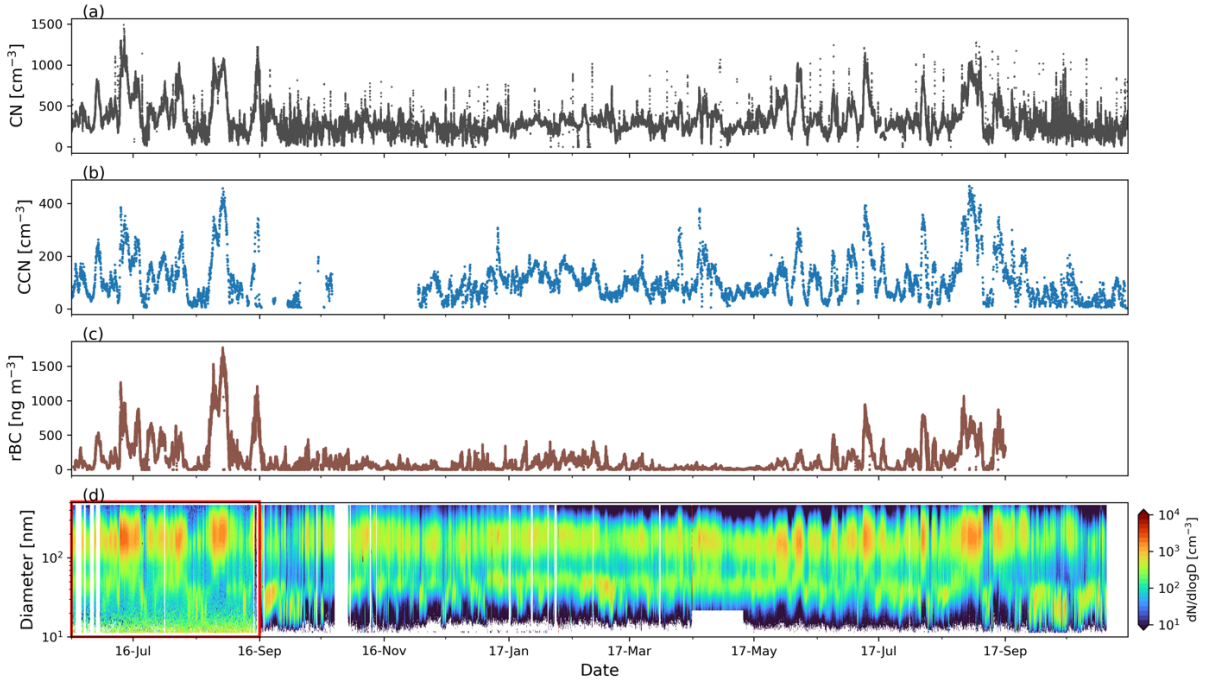

Figure S4. Time series of (a) total particle concentration (CN) measured by the CPC, (b) CCN concentration at 0.1% supersaturation, (c) refractory black carbon (BC) mass concentration measured by the SP2, and (d) particle number size distribution (PNSD) measured by the SMPS.

Figure S4 shows a significant change in SMPS measurements around September 1, 2016. Prior to this date, a higher concentration of ultrafine particles (<20 nm) was observed, whereas after September 1, particles around 10 nm were no longer detected. This abrupt shift suggests a change in SMPS detection capability rather than an actual atmospheric variation.

Since N_{SMPS} is integrated over the 31–1000 nm size range, changes in SMPS performance below 31 nm should have minimal impact on the integrated values. Therefore, it is unlikely that these changes alone explain the observed shifts in correlation. To explore this further, we examined monthly correlations between $N_{CCN1\%}$ and N_{SMPS} throughout the LASIC campaign (Figure S5). During June and July 2016, the correlation followed the Type 1 pattern. In August, the correlation became more scattered and began to show partial signs of the Type 2 pattern; however, this deviation was temporary, as the correlation returned to the Type 1 pattern in September and October. A clear and sustained shift to the Type 2 pattern occurred in November 2016, and this pattern persisted throughout 2017.

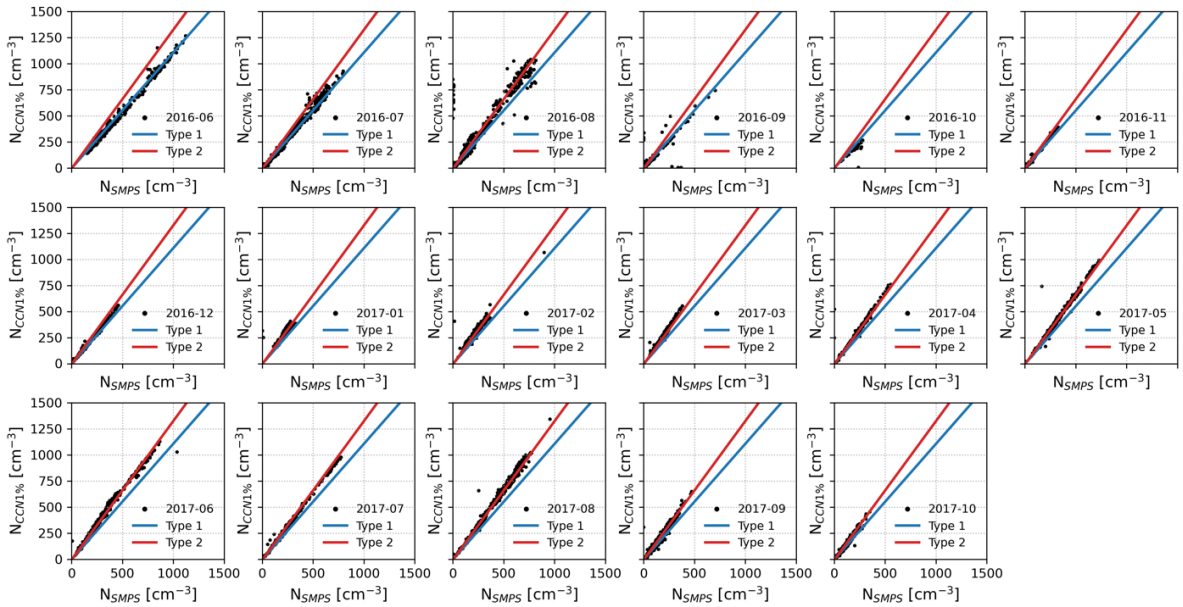

Figure S5. Monthly correlations between the CCN concentration measured at 1% supersaturation ($N_{CCN1\%}$) and the integrated aerosol number concentration from the SMPS (N_{SMPS}, integrated from 31 nm to 1000 nm) throughout the LASIC campaign. The blue and red lines indicate the two distinct correlation patterns (Type 1 and Type 2) discussed in the main text.

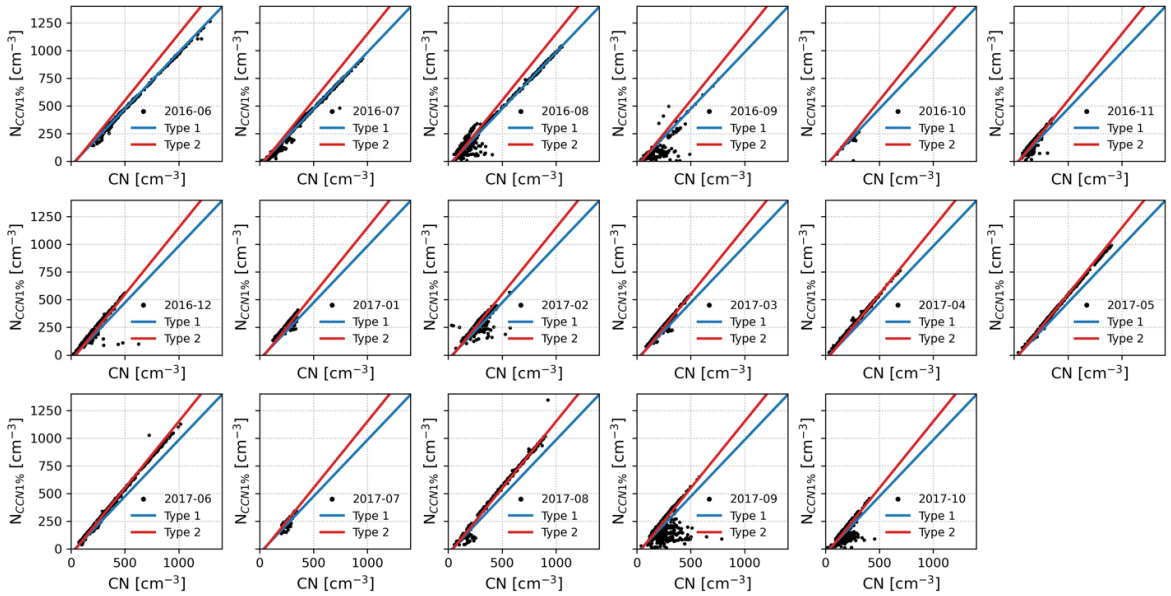

Figure S6. Same as Figure S5 but showing the correlations between $N_{CCN1\%}$ and the CN concentration measured by the CPC (with a cutoff diameter of 10 nm).

To further investigate the source of the correlation shift, we compared $N_{CCN1\%}$ with the total particle concentration (CN) measured by the Condensation Particle Counter (CPC, cutoff at 10 nm), as shown in Figure S6. The correlations between $N_{CCN1\%}$ and CN also shifted from Type 1 to Type 2 around November 2016, closely mirroring the change observed in the $N_{CCN1\%}$–N_{SMPS} relationship. This parallel behavior suggests that the temporary deviation in August 2016 was likely influenced by transient changes in SMPS performance. However, the

sustained shift from November 2016 onward indicates a more permanent instrumental drift or change within the CCN counter itself, rather than an issue specific to the SMPS or CPC.

In summary, the sustained shift in the correlation between $N_{CCN1\%}$ and N_{SMPS} beginning in November 2016 is most likely due to instrumental drift or a permanent alteration in the CCN counter. In contrast, the brief anomaly observed in August 2016 appears to be a transient event, possibly related to short-term variability or temporary SMPS changes.

S3. Estimation of NaCl contribution

To estimate the contribution of sea salt to the observed aerosol hygroscopicity, a closure analysis was performed by comparing the observed κ_{CCN} with the theoretically calculated κ_{chem}, as described in the Methods section. The calculation of κ_{chem} followed the mixing rule outlined by Petters and Kreidenweis (2007), using the densities and κ values of individual aerosol species listed in Table S1.

Table S1. Density and κ value different aerosols species

	$(NH_4)_2SO_4$	NH_4HSO_4	NH_4NO_3	NH_4Cl	OA	H_2SO_4	NaCl	BC
Density (g/cm^3)	1.77 (Haynes et al., 2016)	1.78 (Haynes et al., 2016)	1.72 (Haynes et al., 2016)	1.53 (Haynes et al., 2016)	1.4 (Alfarra et al., 2006)	1.83 Haynes et al., 2016)	2.16 (Haynes et al., 2016)	1.8 (Bond and Bergstrom, 2006)
κ	0.61 (Petters and Kreidenweis, 2007)	0.7*	0.67 (Petters and Kreidenweis, 2007)	1*	0.1 (Zhang et al., 2024)	0.9 (Petters and Kreidenweis, 2007)	1.5* (Zieger et al., 2017)	0 (Petters and Kreidenweis, 2007)

*Note the κ values for NH_4HSO_4 and NH_4Cl are not reported in Petters and Kreidenweis (2007). Therefore, we derived their theoretical values using the following equation (Schulze et al., 2020):

$$\kappa_i = \left(\frac{M_w}{\rho_w}\right)\left(\frac{\rho_i}{M_i}\right)\nu_i$$

where M_w and ρ_w are the molar mass and density of water, respectively, and M_i, ρ_i, and ν_i are the molar mass, density, and van't Hoff factor of the inorganic component. The van't Hoff factor is assumed to be 2.5 for NH_4HSO_4 and 2 for NH_4Cl. The κ of NaCl was too low in Petters and Kreidenweis (2007) and a revised value of 1.5 was used (Zieger et al., 2017).

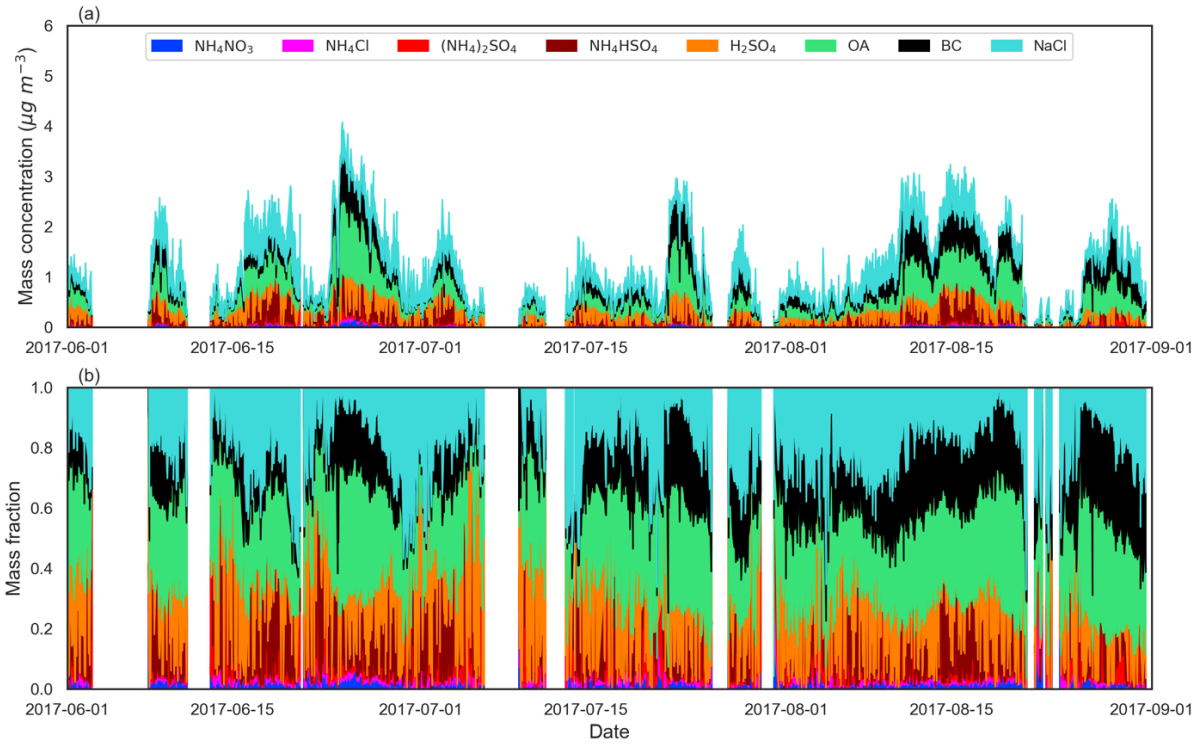

Figure S7. Updated (a) aerosol mass concentration and (b) mass fraction during the fire season in 2017.

The time series of aerosol species, including the estimated NaCl contribution, is shown in Figure S7. A consistently high fraction of H_2SO_4 is observed throughout the fire season. This is due to the measured NH_4^+ concentrations being insufficient to fully neutralize Cl^-, NO^{3-}, and SO_4^{2-} ions. In the absence of measurements for other cations that could balance the excess sulfate, we assigned the unpaired SO_4^{2-} to H_2SO_4. However, other forms of sulfate salts, such as Na_2SO_4, could also be present. To assess the potential impact of using sulfate salts instead of H_2SO_4 on the derived NaCl concentrations, we recalculated the aerosol composition by assigning all excess SO_4^{2-} as Na_2SO_4. The results are shown in Figure S8. The difference between the two assumptions is minimal, as the κ value of H_2SO_4 is 0.9, and that of Na_2SO_4 is 0.8. As a result, this substitution has no significant effect on the derived NaCl concentrations from the κ closure analysis.

It is important to note that H_2SO_4 and $(NH_4)_2SO_4$ do not coexist in the aerosol phase. Although Figure S7 (b) may appear to show both simultaneously, this is due to dense data masking the temporal separation between species. In the calculation, H_2SO_4 only appears when NH_4^+ is insufficient to fully neutralize SO_4^{2-} in the form of NH_4HSO_4. Under these conditions, the excess SO_4^{2-} is represented as H_2SO_4, and $(NH_4)_2SO_4$ is not present.

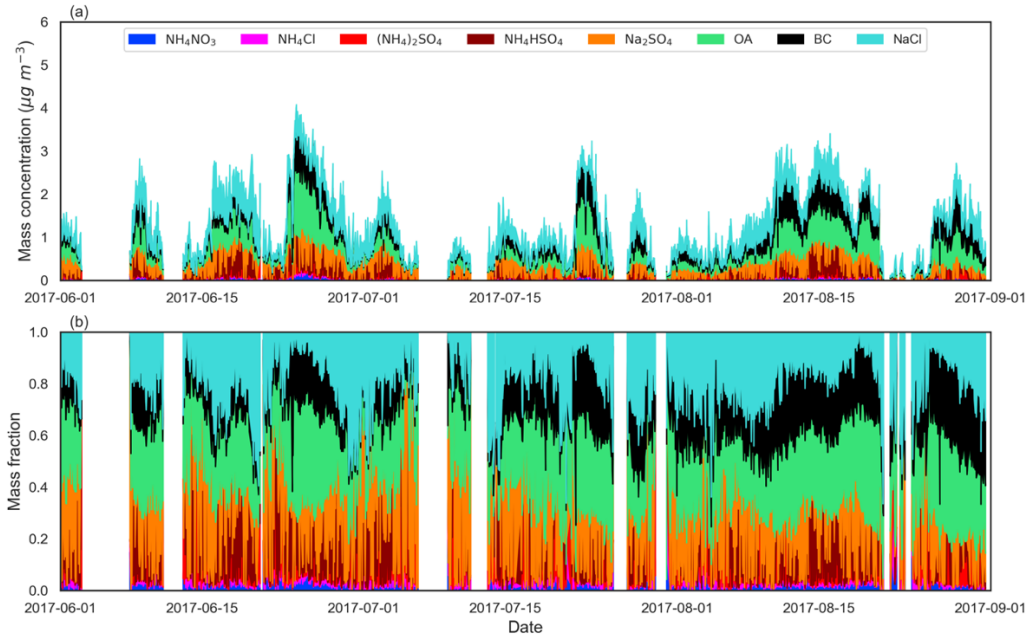

Figure S8. Same as Figure S7, but with excess sulfate represented as Na_2SO_4 instead of H_2SO_4.

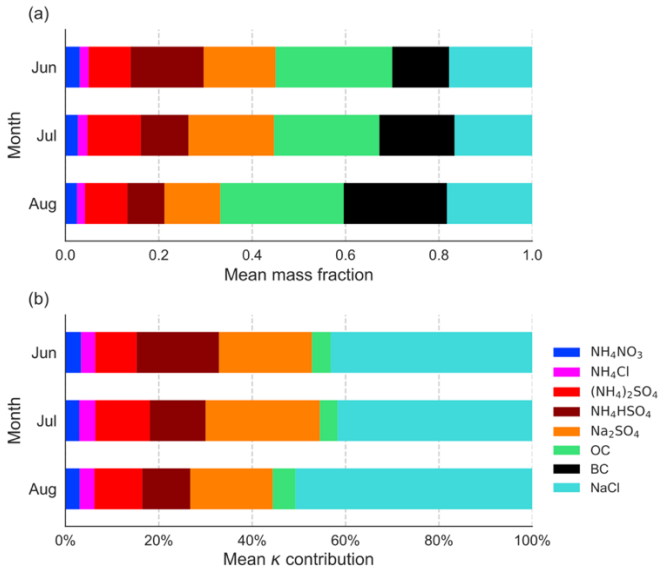

Figure S9**.** Derived monthly mean (a) mass fractions of aerosol species in submicron aerosols (PM_1), and (b) percentage contributions of each aerosol species to the total κ during the 2017 fire season.

Figure S9 shows the monthly mean mass fractions of aerosol species, as well as their contributions to the observed mean κ during the 2017 fire season, under the assumption that excess sulfate represented as Na_2SO_4 instead of H_2SO_4.

Table S2. Elements analyzed and their mean and standard deviation of mass fractions for 231 particles*.

Elements	Particle number	Mean mass fraction (%)	Mass fraction std (%)
Al	231	0.270736	1.238378
Ca	231	0.327576	1.810890
Cl	231	2.174113	6.294387
Co	231	0.005065	0.067790
Cr	231	0.206494	2.794100
F	231	0.016883	0.256601
Fe	231	1.024805	7.862684
K	231	1.746364	3.642440
Mg	231	0.023203	0.204436
N	231	3.353593	7.991303
Na	231	2.195022	4.425461
Ni	231	0.010779	0.163830
O	231	8.925238	8.243104
P	231	0.026970	0.197371
S	231	0.734329	1.765918
Si	231	0.845498	2.288163

*Note, these particles are from the six samples we used in the study, which are Gold8, Gold9, Gold10, Gold14, Gold21, and Gold23.

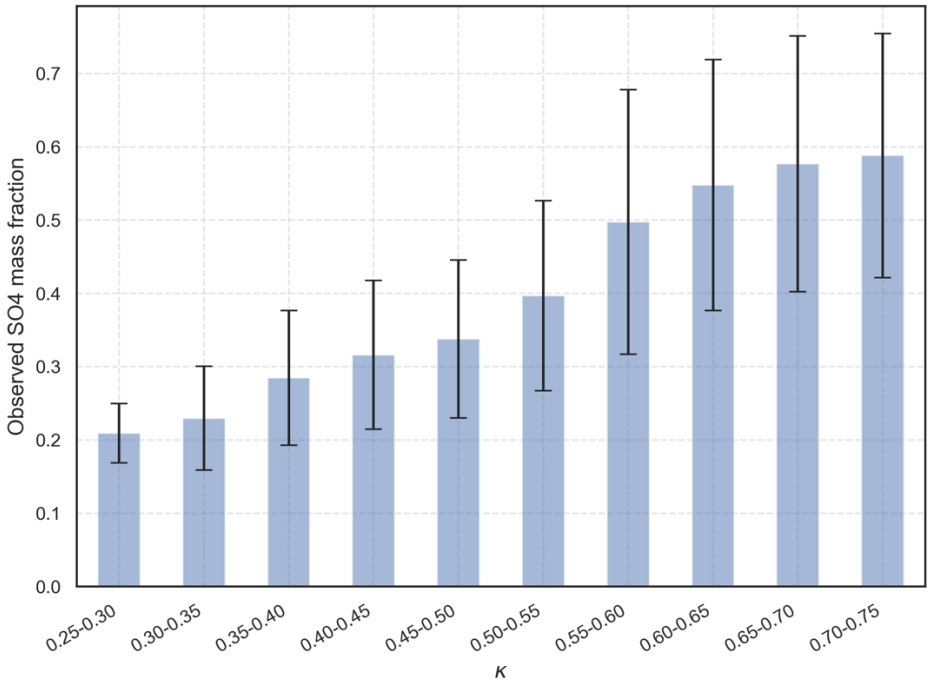

Figure S10. Observed sulfate mass fraction across different κ bins. Error bars represent the standard deviation within each bin.

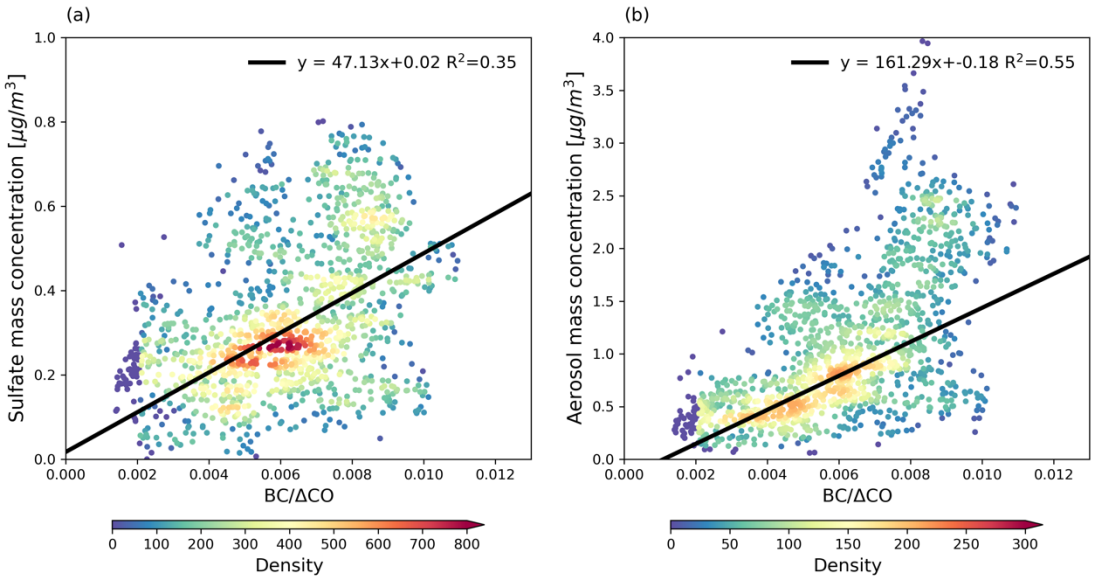

Figure S11. Relationships between BC/ΔCO and (a) the mass concentration of sulfate aerosols, and (b) the total mass of aerosol particles during the BB season in 2017, where the total mass is the sum of the species observed by ACSM and BC measured by SP2. The black lines represent linear regressions, with the corresponding equations displayed in the legend. The color scale indicates data density, represented as the count of data points within gridded 50x50 bins.

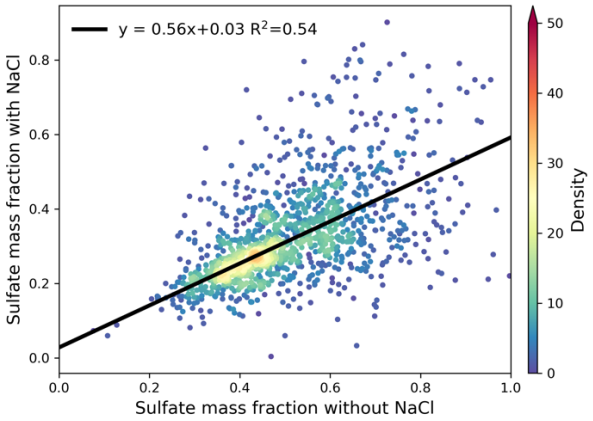

Figure S12. Relationship between sulfate mass fraction in observed aerosols without NaCl (sea-salt-free) and estimated sulfate mass fraction in aerosols containing NaCl in 2017. Colors indicate data density, representing the number of data points within each grid cell (divided into 40×40 bins across the data range). Solid black lines show linear regression fits, with corresponding regression equations provided in the legend.

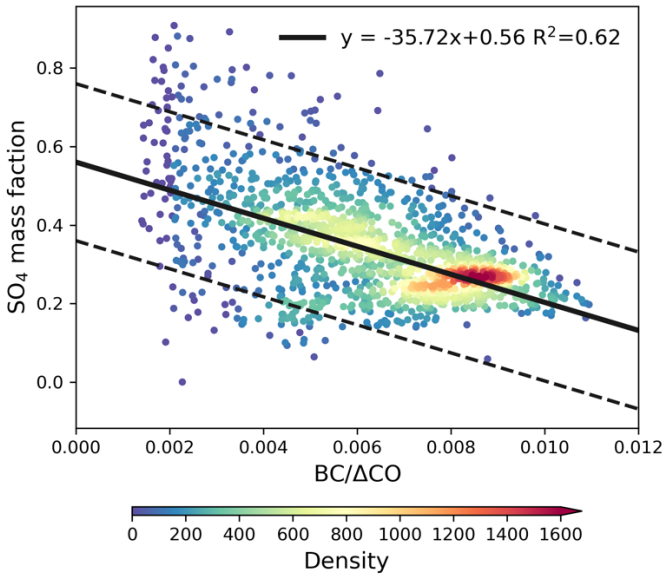

Figure S13. Relationship between BC/ΔCO and sulfate mass fraction in 2017. Colors represent data density, defined as the number of data points within each grid cell (50×50 bins across the data range). Solid black lines indicate linear regression fits, with corresponding equations provided in the legend. Dashed lines indicate lower and upper bounds of regression fits derived from data points exceeding a density threshold of 200.

Reference

Alfarra, M. R., Paulsen, D., Gysel, M., Garforth, A. A., Dommen, J., Prévôt, A. S. H., Worsnop, D. R., Baltensperger, U., and Coe, H.: A mass spectrometric study of secondary organic aerosols formed from the photooxidation of anthropogenic and biogenic precursors in a reaction chamber, Atmospheric Chemistry and Physics, 6, 5279–5293, https://doi.org/10.5194/acp-6-5279-2006, 2006.

Bond, T. C. and Bergstrom, R. W.: Light Absorption by Carbonaceous Particles: An Investigative Review, Aerosol Science and Technology, 40, 27–67, https://doi.org/10.1080/02786820500421521, 2006.

Haynes, W. M., Lide, D. R., and Bruno, T. J.: CRC Handbook of Chemistry and Physics: A Ready-reference Book of Chemical and Physical Data, 2016th–2017th, 97th Edition ed., CRC Press, 2016.

Petters, M. D. and Kreidenweis, S. M.: A single parameter representation of hygroscopic growth and cloud condensation nucleus activity, Atmospheric Chemistry and Physics, 7, 1961–1971, https://doi.org/10.5194/acp-7-1961-2007, 2007.

Schulze, B. C., Charan, S. M., Kenseth, C. M., Kong, W., Bates, K. H., Williams, W., Metcalf, A. R., Jonsson, H. H., Woods, R., Sorooshian, A., Flagan, R. C., and Seinfeld, J. H.: Characterization of Aerosol Hygroscopicity Over the Northeast Pacific Ocean: Impacts on Prediction of CCN and Stratocumulus Cloud Droplet Number Concentrations, Earth and Space Science, 7, e2020EA001098, https://doi.org/10.1029/2020EA001098, 2020.

Zhang, L., Segal-Rozenhaimer, M., Che, H., Dang, C., Sun, J., Kuang, Y., Formenti, P., and Howell, S. G.: Aerosol hygroscopicity over the southeast Atlantic Ocean during the biomass burning season – Part 1: From the perspective of scattering enhancement, Atmospheric Chemistry and Physics, 24, 13849–13864, https://doi.org/10.5194/acp-24-13849-2024, 2024.

Zieger, P., Väisänen, O., Corbin, J. C., Partridge, D. G., Bastelberger, S., Mousavi-Fard, M., Rosati, B., Gysel, M., Krieger, U. K., Leck, C., Nenes, A., Riipinen, I., Virtanen, A., and Salter, M. E.: Revising the hygroscopicity of inorganic sea salt particles, Nat Commun, 8, 15883, https://doi.org/10.1038/ncomms15883, 2017.